Modeling Fluid-Structure Interaction of Biodegradation in Engineered Tissue Scaffolds

P. Patki[1], F. Costanzo[2]
1. Mechanical Engineering Department, The Pennsylvania State University, University Park, PA, USA
2. Center for Neural Engineering, The Pennsylvania State University, University Park, PA, USA

1. Introduction

Nerve injuries or breakage caused by bullet wounds or accidents often lead to loss of sensitivity, or motion, or both, in the injured organ. The human body has inherent mechanism to repair such injured or broken nerves. Fibers emerge from the ends of the broken nerve and join to recover the nerve. However, when the gap between the broken nerve ends is large, misalignment of the rejoining fibers can hinder the healthy recovery of the broken nerve. Hence, in order to assist the recovery of such nerves, external support is provided in the form of surgical implants known as nerve regeneration scaffolds or Tissue Engineered Nerve Guides (TENGs) [1, 2]. These sleeve-like structures often have embedded drugs and nutrients and are typically porous to allow the supply of drugs and nutrients to the recovering nerve ends. They not only provide alignment to the re-growing nerve fibers, but also provide mechanical support to it. Fig. 1 shows a typical TENG. Moreover, in order to avoid surgery for the removal of these TENGs after the complete recovery of the nerve, biodegradability is a desirable property of the scaffold. Ideally, the degradation rate of the scaffold should equal the rate of recovery of the nerve.

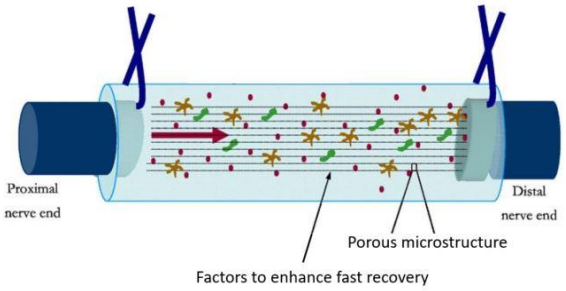

Figure 1. A typical nerve guidance channel, [2].

Thus, the design of these nerve regeneration scaffolds requires a careful study of their degradation rates and how their transport and mechanical properties evolve as they degrade. In this paper, we describe a mathematical formulation which we have developed to describe this complex coupling between the chemistry-mechanics-transport of the scaffold material, and the FEM implementation of it in COMSOL® Multiphysics.

When inserted in the body, blood and other such bodily fluids are expected to flow past the porous scaffold. Thus, studying the mechanics of the solid also requires the study of fluid-structure interaction of the solid and the surrounding base fluid. The base fluid also plays an important role in the initiation of the degradation reaction through hydrolysis [3]. Thus, the reduced mechanism of the degradation chemistry of the scaffold is expected to consist of three components: the poro-elastic solid scaffold, the product of the degradation reaction, and the base fluid. Mixture theory is a continuum framework for the study of behavior of all the components in a mixture. Thus, for the study of our three-component system, we choose this mathematical framework for the derivation of our governing equations. Previous studies mostly focus on the extreme cases in which there is significant difference in the order of time scale of diffusion and chemistry (c.f. [4, 5]). The asymptotic cases derived in these studies are applicable to extreme cases involving either very rapid or very slow chemistries. We rather derive a more general theory which is applicable to any combination of chemistry-diffusion time scales and can be later specialized according to the specific case.

In this paper we discuss the COMSOL® Multiphysics implementation of the Finite Element Method (FEM) based numerical framework based on the derived mathematical model. The weak formulation of the partial differential equations (PDE)s has been implemented using Weak form PDE interface within the Mathematics module of COMSOL®. The stability and accuracy of the numerical framework is tested using the Method of Manufactured Solutions (MMS).

The paper is organized as follows: Next section describes the basics of mixture theory and briefly describes the governing equations conditions for the fluid-structure interaction and degradation of the porous scaffolds. Section 3 describes the COMSOL® implementation of the resultant numerical model along with a discussion on the accuracy of the numerical scheme as tested using MMS. Finally, we summarize our important results in the last section.

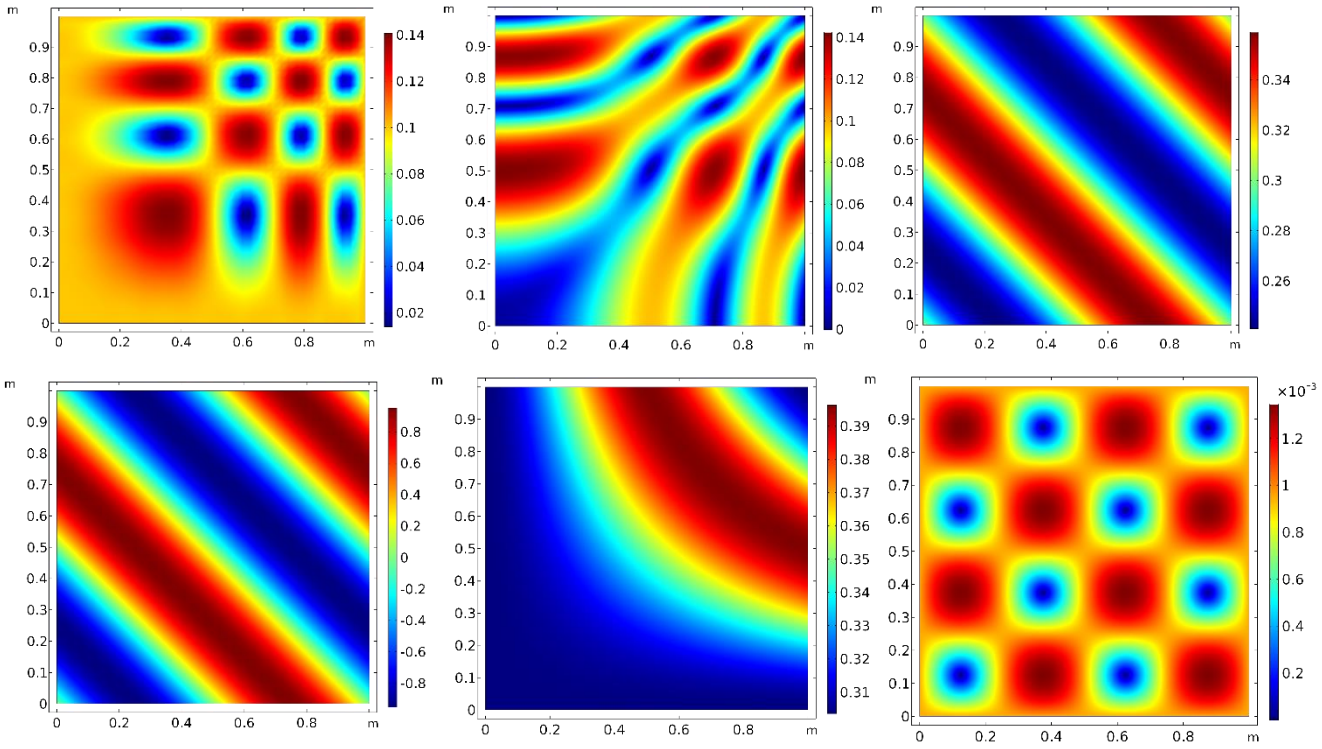

Figure 2. Manufactured Solutions for different variables. (*From left to right) Top row:* $||\mathbf{v}_{\mathbf{fil}_1}||$, $||\mathbf{v}_{\mathbf{fil}_2}||$, $\boldsymbol{\phi}_s$; *Bottom row:* $\boldsymbol{p}$, $\boldsymbol{\phi}_1$, $||\mathbf{u}_s||$.

2. Mathematical Model

2.1 Basics of mixture theory – kinematics and balance laws, [6]:

For a mixture comprising of N components, we assume that all the constituents co-exist at any given point in the domain. The mass density of the pure constituent a (mass of constituent a per unit volume of the constituent) and its mass density as perceived in the mixture (mass of constituent a per unit mixture volume) are denoted by γ_a and ρ_a respectively. The volume fraction of a component a in the mixture, defined as the volume occupied by the component divided by the total volume of the mixture, is denoted by ϕ_a. The assumption that the constituents of the mixture occupy the volume of the mixture, leads to the 'saturation constraint', which is given by,

$$\sum_1^N \phi_a = 1. \qquad (1)$$

The relationship between ϕ_a, γ_a and ρ_a is given by,

$$\rho_a = \gamma_a \phi_a. \qquad (2)$$

The velocity of any component a in the mixture is denoted by $\mathbf{v}_a$. The balance of mass for any component a in the mixture is then given by,

$$\frac{\partial \rho_a}{\partial t} + \nabla \cdot (\rho_a \mathbf{v}_a) = \hat{c}_a, \qquad (3)$$

where $\hat{c}_a$ denotes the rate of production or consumption of component a due to chemical reactions.

Balance of momentum equation for the component a is given by,

$$\rho_a\left(\frac{\partial \mathbf{v}_a}{\partial t} + \nabla \mathbf{v}_a \cdot \mathbf{v}_a\right) = \nabla \cdot \mathsf{T}_a + \rho_a \mathbf{b}_a + \hat{\mathbf{p}}_a, \qquad (4)$$

where T_a and $\mathbf{b}_a$ are the stress tensor and body force vector for the constituent a. The vector $\hat{\mathbf{p}}_a$ is the force of interaction of the constituent a with all other constituents in the mixture.

2.2 Constitutive relations and final form of governing equations for a degrading scaffold embedded in a fluid bath

For our mixture comprising of the poro-elastic degrading solid, base fluid and degradation product, we derived the constitutive forms for T_a and $\hat{\mathbf{p}}_a$, to obtain the system of governing equations. The product of degradation is assumed to be a fluid. Under the assumption that the inertia effects can be ignored (i.e. acceleration terms can be ignored), the final form of the governing equations for the fluids and the poro-elastic solid are obtained as,

$$\mathbf{0} = -\phi_f \nabla p + \gamma_f \phi_f \mathbf{b}_f - \phi_f \frac{\mu_f}{\kappa_s} \mathbf{v}_{\mathrm{fil}_f}, \quad (5)$$

$$\mathbf{0} = -\phi_s \nabla p + \gamma_s \phi_s \mathbf{b}_s + \sum_{f=1}^{2} \phi_f \frac{\mu_f}{\kappa_s} \mathbf{v}_{\mathrm{fil}_f} + \nabla \cdot \mathsf{T}^e - \sum_{f=1}^{2} \hat{c}_f \mathbf{v}_f - \hat{c}_s \mathbf{v}_s, \quad (6)$$

Here, *f* denotes fluid components, and *s* denotes solid. The term p denotes the hydrostatic pressure which appears in the momentum balance equation of all constituents. T^e denotes the first Piola-Kichhoff stress tensor corresponding to the elastic stress tensor for the solid. The terms μ_f and κ_s are the fluid viscosity and permeability of the porous solid, respectively. Another term that appears in Eqs. (5) and (6) is $\mathbf{v}_{\mathrm{fil}_f}$, which is known as the 'filtration velocity' for fluids, and is the relative velocity of the fluid with respect to the solid, scaled by the fluid volume fraction, and is given by,

$$\mathbf{v}_{\mathrm{fil}_f} = \phi_f (\mathbf{v}_f - \mathbf{v}_s). \quad (7)$$

The subscript *f* takes values 1 and 2 and for the base fluid and degradation product, respectively. We model the elastic response of the solid as Neo-Hookean. Eqs. (5) and (6) are written in Eulerian form. Since our problem involves a solid and fluids, these equations were converted into an arbitray Lagrangian- Eulerian framework and were then implemented in an FEM model. The model has similar structure for the non-reactive flow through porous media model as presented in [7].

3. FEM model implementation using COMSOL® Multiphysics

3.1 Problem setup

Our system of equations for the three-component mixture involves 8 PDEs: 3 mass balance equations, 3 momentum balance equations and a kinematic relationship between solid displacement and solid velocity (which is essential for the term involving the term T^e). We solve these 8 equations simultaneously for 8 variables: velocities for each of the three constituents, volume fractions (or densities) of each constituent, solid displacement and pressure.

The Mathematics module of COMSOL® Multiphysics provides an excellent framework for the testing of FEM-based numerical frameworks. We tested our FEM model with the help of 'Method of Manufactured Solutions' (c.f. [8]) on a 2D square domain of side 1m. 'Solutions' were assigned to each variable, and the corresponding Dirichlet boundary conditions and source terms were derived for every variable in the system. The resultant system of equations was solved with the derived boundary conditions, and the solutions were tested against the imposed manufactured solution to test for accuracy of the numerical system. The manufactured solutions for various variables are as follows:

$$\mathbf{u}_s = \overline{u}_s \sin\left(\frac{2\pi t}{t_0}\right)\left[\cos\left(2\pi \frac{x+y}{L}\right)\hat{\mathbf{i}} + \sin\left(2\pi \frac{x-y}{L}\right)\hat{\mathbf{j}}\right],$$

$$\mathbf{v}_{\mathrm{fil}_1} = \overline{v}_{\mathrm{fil}_1} \cos\left(\frac{2\pi t}{t_0}\right)\left[\sin\left(2\pi \frac{x^2+y^2}{L^2}\right)\hat{\mathbf{i}} + \cos\left(2\pi \frac{x^2-y^2}{L^2}\right)\hat{\mathbf{j}}\right],$$

$$\mathbf{v}_{\mathrm{fil}_2} = \overline{v}_{\mathrm{fil}_2} \cos\left(\frac{2\pi t}{t_0}\right)\left[\cos\left(2\pi \frac{x^2}{L^2}\right)\sin\left(2\pi \frac{y^2}{L^2}\right)\hat{\mathbf{i}} + \sin\left(2\pi \frac{x^2-y^2}{L^2}\right)\hat{\mathbf{j}}\right],$$

$$p = \overline{p} \sin\left(\frac{2\pi t}{t_0}\right)\sin\left(2\pi \frac{x+y}{L}\right),$$

$$\phi_1 = \check{\phi}_1 + \overline{\phi}_1 \cos\left(\frac{2\pi t}{t_0}\right)\cos\left(2\pi \frac{x+y}{L}\right),$$

$$\phi_s = \check{\phi}_s + \overline{\phi}_s \sin\left(\frac{2\pi t}{t_0}\right)\sin\left(2\pi \frac{x+y}{L}\right).$$

The constant values are: L = 1m and t_0 = 1s. All the simulations were run as 'time dependent' for a total time of 1s. Referring to Eqs. (5) and (6), the values of fluid viscosities for the base fluid and degradation product, μ_1 and μ_2; and solid permeability, κ_s were chosen as 0.001 kg/s.m, 0.0015 kg/s.m and 0.001m^2 respectively. In order to capture various degradation rates, various combinations of the constants $\check{\phi}_1$, $\check{\phi}_s$, $\overline{\phi}_1$ and $\overline{\phi}_s$ were chosen, as given in Table 1. Fig. 2 shows the typical nature of manufactured solutions that were employed for various variables. The solution is obtained using a mesh of size h = L/128, at time = 0.7s. We chose a uniform swept mesh for our analysis, with square elements. For testing the accuracy, we used a parametric sweep over the mesh size. The mesh sizes we used were $1/2^n$ m, where the n was sequentially chosen as 8, 16, 32, 64, 128.

Table 1: Constants for manufactured solutions of volume fractions.

Case	$\check{\phi}_1$	$\overline{\phi}_1$	$\check{\phi}_s$	$\overline{\phi}_s$
1	0.2	0.1	0.1	0.1
2	0.35	0.15	0.3	0.1
3	0.2	0.1	0.5	0.2

3.2 Solver and shape function specifications:

For the time stepping, we implemented implicit time marching using the variable-order variable time step backward difference formula (BDF) (c.f. [9]). The BDF order was restricted between 2 and 5, and a maximum time step size of 0.001s was imposed. The resultant non-linear system of equations for every time step was solved using Newton's method (with no damping). For the termination criterion for the iterations, we used minimum relative tolerance of 0.001. The linear solver PARDISO ([10-12]) was employed for the linear system of equations. Since the numerical system is expected to suffer from stability issues, the Brezzi-Babuska condition ([13, 14],) was invoked, wherein two combinations of shape functions for the vectors (velocities and solid displacement) and pressure were chosen:

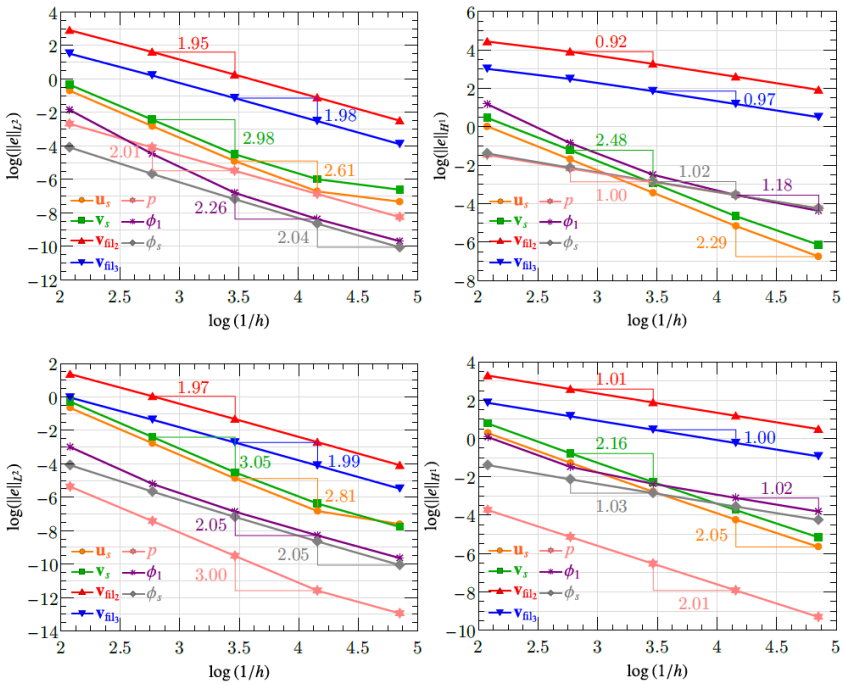

Figure 3: L^2 and H^1 error norms for the case 3 described in Table 1.

- Lagrange quadratic shape functions for vectors and Lagrange linear shape functions for pressure.
- Lagrange cubic shape functions for vectors and Lagrange quadratic shape functions for pressure.

Lagrange linear shape functions were used for the volume fractions.

4. Numerical results

Results for the numerical problem and parameter values described in the previous section are presented in this section. The stability of the numerical scheme was observed to be dependent on the relative filtration velocity with respect to the solid. In order to study the stability behavior, the solid displacement amplitude, $\overline{u}_s$ was fixed as 0.01m, and three values of the filtration velocity magnitudes, $\overline{v}_{\mathrm{fil}_1}$ and $\overline{v}_{\mathrm{fil}_2}$ were considered: 0.01m/s, 0.1m/s and 1m/s. It was observed that stable numerical solutions were obtained, even without any additional stabilization terms, for filtration velocity magnitudes of 0.01m/s and 0.1m/s. Also, the numerical model failed when the volume fractions went above a value of 0.8, or below 0.1.

Without loss of generality, convergence rates (L^2 and H^1 error norms) for the case 1 in Table 1 are shown in Fig. 3 for $\overline{v}_{\mathrm{fil}_1} = \overline{v}_{\mathrm{fil}_2} = 0.01$ m/s, and for time = 0.7 s. The L^2 error norms and H^1 semi-norms for the filtration velocities are around 2 and 1 respectively, and for the solid displacement and velocity are around 2.6 and 2 respectively for both the combinations of shape functions. Similarly, the L^2 and H^1 error norms for the volume fractions are around 2 and 1 irrespective of the combination of shape functions. The error norms for pressure, however, are observed to be dependent on the order of interpolation function: the L^2 error norms are around 2 and 3 for Lagrange linear and quadratic pressure shape functions respectively, whereas the H^1 semi-norms are around 1 and 2 respectively. Similar trends for convergence rates are observed for all the other cases in Table 1, and for filtration velocity amplitudes of 0.1m/s. For the case when $\overline{v}_{\mathrm{fil}_1} = \overline{v}_{\mathrm{fil}_2} = 1$m/s, the convergence rates become more erratic, and the convergence becomes harder to achieve at higher resolutions.

5. Conclusions

In this paper, we present a mathematical formulation which we have derived based on principles of mixture theory, to capture the bio-degradation of poro-elastic polymers and corresponding evolution of their mechanical and transport properties. An FEM based numerical model has been derived based on the

mathematical model. The FEM model has been implemented in COMSOL® Multiphysics using the Weak form PDE interface of the Mathematics module. The model has been tested using the method of manufactured solutions for convergence and stability. Except for cases when the volume fractions are below 0.1 or above 0.8, and when the filtration velocities are of the order 1m/s and above, for a solid displacement magnitude of 0.001m, the FEM model is observed to be stable, for two different combinations of shape functions which were chosen so as to satisfy the Brezzi-Babuska condition. Future research would focus on the application of the model to simulate scenarios involving insertion of the scaffolds in real bio-medical simulations.

References

1. Mahesh C. Dodla, Melissa Alvarado-Velez, Vivek J. Mukhatyar, and Ravi V. Bellamkonda. Chapter 69 - peripheral nerve regeneration. In *Principles of Regenerative Medicine* (Third Edition), 1223 - 1236. Academic Press, Boston, (2019).

2. Ravi V Bellamkonda. Peripheral nerve regeneration: an opinion on channels, scaffolds and anisotropy. *Biomaterials*, **27(19)**, 3515-3518, 2006.

3. Ying Wang, Jingzhe Pan, Xiaoxiao Han, Csaba Sinka, and Lifeng Ding. A phenomenological model for the degradation of biodegradable polymers. *Biomaterials*, **29(23)**: 3393-3401, 2008.

4. Xiaoxiao Han and Jingzhe Pan. A model for simultaneous crystallisation and biodegradation of biodegradable polymers. *Biomaterials*, **30(3)**: 423-430, 2009.

5. Satish Karra and KR Rajagopal. A model for the thermo-oxidative degradation of polyimides. *Mechanics of Time-Dependent Materials*, **16(3)**: 329-342, 2012.

6. Ray M. Bowen. *Theory of mixtures In Continuum physics*, 3, 1976.

7. Ray M. Bowen. Incompressible porous media models by use of the theory of mixtures. *International Journal of Engineering Science*, **18(9):** 1129-1148, 1980.

8. Kambiz Salari and Patrick Knupp. Code verifcation by the method of manufactured solutions. Technical report, Sandia National Labs., Albuquerque, NM (US); Sandia National Labs, 2000.

9. COMSOL Multiphysics® v.5.3 Reference Manual.

10. Andrey Kuzmin, Mathieu Luisier, and Olaf Schenk. Fast methods for computing selected elements of the green's function in massively parallel nanoelectronic device simulations. In Euro-Par 2013 Parallel Processing, 533-544, Berlin, Heidelberg, 2013. Springer Berlin Heidelberg.

11. Olaf Schenk, Matthias Bollhöfer, and Rudolf A Römer. On large-scale diagonalization techniques for the anderson model of localization. SIAM review, **50(1)**: 91-112, 2008.

12. Olaf Schenk, Andreas Wächter, and Michael Hagemann. Matching-based preprocessing algorithms to the solution of saddle-point problems in large-scale non-convex interior-point optimization. *Computational Optimization and Applications*, **36(2)**: 321-341, Apr 2007

13. Brezzi, Franco, and Michel Fortin. *Mixed and hybrid finite element methods*. **15**, Springer Science & Business Media, 2012.

14. F. Costanzo and S. T. Miller. An arbitrary Lagrangian-Eulerian finite element formulation for a poro-elasticity problem stemming from mixture theory. *Computer Methods in Applied Mechanics and Engineering*, **323**: 64-97, 2017.

Acknowledgements

We gratefully acknowledge partial support by the National Science Foundation through grant CMMI 1537008.